Nano Res (2010) 3: 281–287
DOI 10.1007/s12274-010-1031-3
Research Article

Ultraviolet Photoconductance of a Single Hexagonal WO_3 Nanowire

Kai Huang[1], Qing Zhang[1] (✉), Feng Yang[2], and Deyan He[2]

[1] Microelectronics Center, School of Electrical and Electronics Engineering, Nanyang Technological University, Singapore 639798
[2] School of Physical Science and Technology, Lanzhou University, Lanzhou 730000, China

Received: 24 November 2009 / Revised: 10 January 2010 / Accepted: 19 February 2010

ABSTRACT

The ultraviolet (UV) photoconductance properties of a single hexagonal WO_3 nanowire have been studied systematically. The conductance of WO_3 nanowires is very sensitive to ultraviolet B light and a field-effect transistor (FET) nanodevice incorporating a single WO_3 nanowire exhibits excellent sensitivity, reversibility, and wavelength selectivity. A high photoconductivity gain suggests that WO_3 nanowires can be used as the sensing element for UV photodetectors. Measurements under UV light in vacuum show that the adsorption and desorption of oxygen molecules on the surface of the WO_3 nanowire can significantly influence its photoelectrical properties. The WO_3 nanowires have potential applications in biological sensors, optoelectronic devices, optical memory, and other areas.

KEYWORDS

Hexagonal WO_3 nanowire, ultraviolet, photodetector

Since discovery of ultraviolet (UV) radiation, the applications of UV light in biotechnology, medical applications, astronomy, and materials science research have been an active research area [1]. In these activities, much attention has been paid to the issue of the safety of UV radiation. UV irradiation of human bodies can damage DNA structure, suppress the immune system, and increase skin photoaging, leading to an increasing number of cancer cases [2]. Therefore, high-efficiency and low-energy consumption UV detectors are in high demand. Nano-photodetectors based on one-dimensional wide bandgap semiconductor materials in the form of nanowires, nanotubes, or nanofibers have been demonstrated to have very attractive performances due to the low dimensions and large surface-to-volume ratios of such nanomaterials [3–6]. To date, photoconductance based on wide bandgap semiconductors, for example, GaN, ZnO, Ga_2O_3, and Si_3N_4 nanostructures, has been employed for UV detection [7–10].

Tungsten oxide (WO_3), a very important type of semiconductor material, has been extensively investigated due to its promising physical and chemical properties [11–14]. By virtue of its outstanding electrochromic, optochromic, and gasochromic properties, in the past few decades WO_3 has been used to manufacture various devices such as flat-panel displays, electrochromic "smart" windows, optical modulation devices, write–read–erase optical devices, gas sensors, and field emission devices [15–17]. WO_3 is a potential material for detecting UV radiation because it has an indirect large energy band gap

Address correspondence to eqzhang@ntu.edu.sg

[18, 19]. In this paper, we present a systematic study of the UV photoconductive characteristics of a single WO_3 nanowire in order to explore its potential for applications in high-sensitivity UV photodetection. We find that the conductivity of the WO_3 nanowires is extremely sensitive to UV light exposure. UV photocurrent to dark current ratios of several orders of magnitude, high response speeds, and excellent stability and reproducibility suggest that these WO_3 nanowires could serve as the sensing element for high-sensitivity UV light detectors and optical switching devices for nanoscale optoelectronic applications.

The WO_3 nanowires were synthesized by a simple hydrothermal method using Na_2SO_4 as a structure-directing agent [20]. Examination by field-emission scanning electron microscopy (SEM, Hitachi S-4800) revealed that the resulting products are composed of uniform nanowires with diameters in the range 100–200 nm, and lengths of up to ~5 μm, and no other products can be found, as shown in Figs. 1(a) and 1(b). A high-resolution transmission electron microscopy (HRTEM, JEM 2100, 200 KV) image (Fig. 1(c)) and X-ray diffraction (XRD Philip, PANalytical, X'Pert PRO) pattern (Fig. 1(d)) indicated that the WO_3 nanowires are hexagonal (h-WO_3) single crystals oriented along the [001] direction, in contrast to the monoclinic nanostructure of tungsten oxides synthesized by thermal treatment [21], solvothermal synthesis [22], and CVD processes [23].

To characterize the electrical properties of the nanowires, a single nanowire was assembled into a field-effect transistor (FET) device. The device was fabricated using e-beam lithography. Seven parallel Ti/Au (10 nm/200 nm) electrodes spaced about 2 μm apart were fabricated on a single WO_3 nanowire. The UV photoconductivity measurements were performed with UV illumination (Spectroline handheld E-Series) and an Agilent B1500A Semiconductor Device Analyzer. The source–drain current–voltage (I_{sd}–V_{sd}) plot of a WO_3 nanowire FET device at different gate voltages is shown in Fig. 2(a). The conductance of the h-WO_3 nanowire increases with increasing gate voltage,

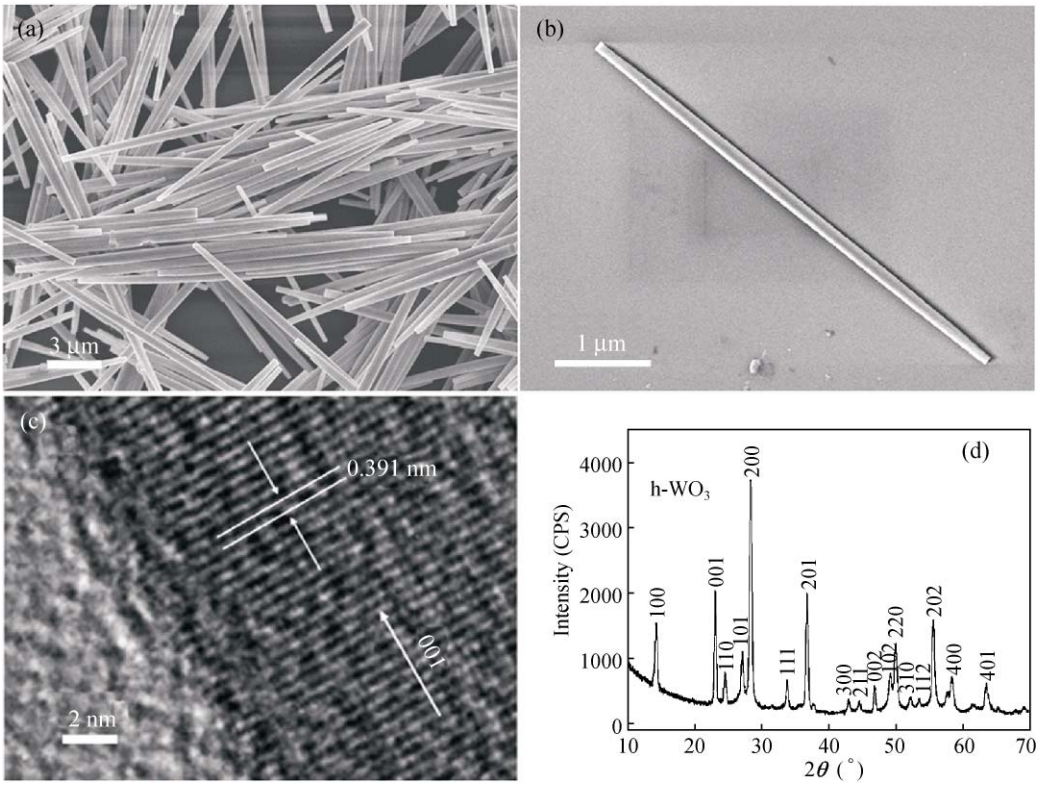

Figure 1 (a) SEM images of as-synthesized WO_3 nanowires. (b) Higher-magnification SEM images of one typical single nanowire. (c) HRTEM image of a single WO_3 nanowire. Note that the nanowire axis is along the [001] direction, and the fringe spacing of 0.391 nm corresponding the (001) lattice spacing of hexagonal WO_3 is denoted. (d) XRD pattern of the synthesized product

which indicates that these nanowires are intrinsic n-type. This n-type behavior in nominally undoped tungsten oxide is believed to result from oxygen vacancies. The inset in Fig. 2(a) shows an SEM image of the WO_3 single nanowire device. Figure 2(b) shows typical *I*–*V* curves obtained when the nanodevices were exposed to UV light with wavelengths of 254 nm, 312 nm, and 365 nm at a constant light intensity of 2 mW/cm². These results show that the photoconductance ($G_{pc} = I/V$) is sensitive to the excitation wavelength, with the photoconductance being 2, 15, and 8 nS for irradiation at 365, 312, and 254 nm, respectively. In the dark state, the WO_3 nanowire was highly insulating, and the linear *I*–*V* curve (in the inset of Fig. 2(b)) shows the ohmic contacts of the WO_3 nanowire with the Au electrodes; the dark conductance was only 0.1 nS. These results indicate that our WO_3 nanowires devices have a high photosensitivity to ultraviolet light with wavelengths in the UVB region from 280 nm to 320 nm and exhibit an excellent wavelength selectivity. As a comparison, we measured the current flowing between the Au electrodes without any nanowires and found no detectable current under UV illumination. Thus, we can confirm that the both photoconductance and dark conductance really arise from the WO_3 nanowire itself, instead of from the electrodes and substrates.

To clarify the origin of the spectral response, the absorption spectra for the WO_3 nanowires were measured, as shown in Fig. 2(c). The optical absorption near the energy band edge for a semiconductor is described by the following Eq. (24):

$$ahv = A(hv - E_g)^{n/2} \quad (1)$$

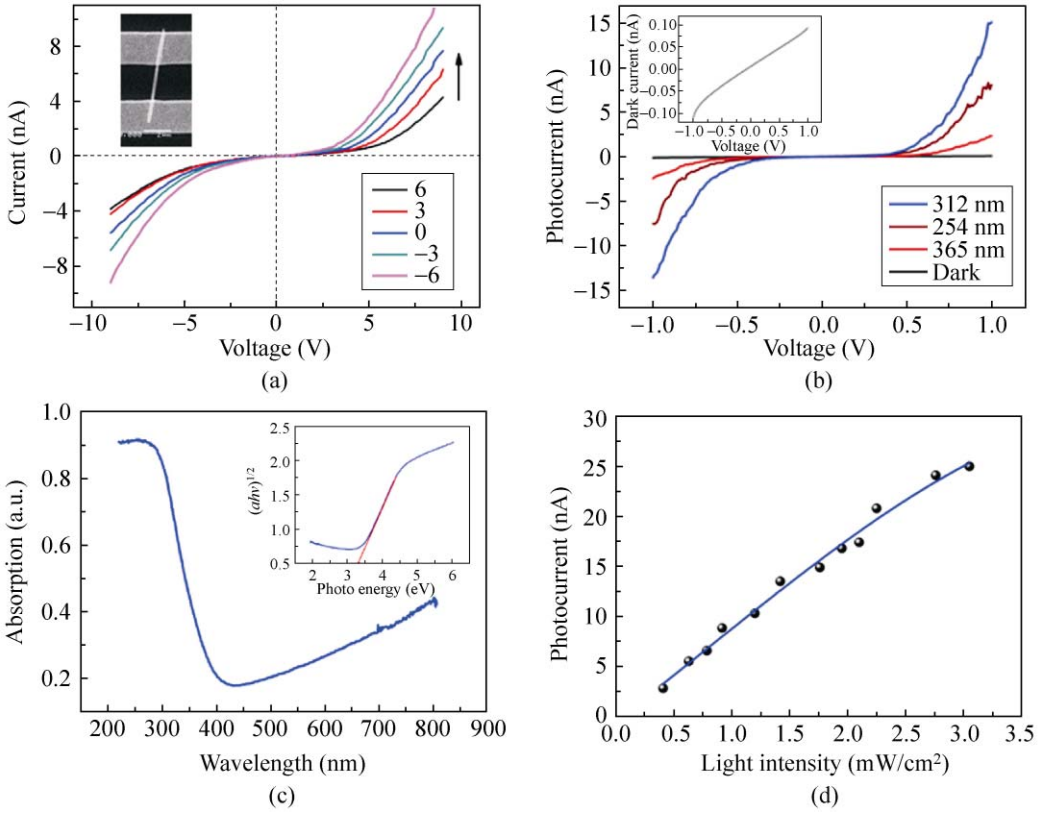

Figure 2 (a) I_{ds}–V_{ds} curves of a single WO_3 nanowire at different gate voltages. Inset is an SEM image of a single WO_3 nanowire device. (b) The *I*–*V* curves of a single WO_3 nanowire illuminated under different wavelengths. The light intensity is kept constant at 2 mW/cm². The inset shows an enlarged view of the *I*–*V* curve measured in the dark state. (c) The UV–vis absorption spectrum of as-prepared WO_3 nanowires. The inset is a plot of the $(ahv)^{1/2}$ versus photon energy (hv). (d) Photocurrent at different light intensities under illumination by 312 nm UV light with a bias voltage of 1 V

where a, v, E_g, and A are the absorption coefficient, light frequency, energy band gap, and a constant, respectively, and n depends on whether the transition is direct ($n = 1$) or indirect ($n = 4$). The intercept with the hv axis of the tangent to the curve of $(ahv)^{1/2}$ plotted against hv gives a good approximation of the energy band gap (i.e., E_g is ~ 3.30 eV), seen from the inset of Fig. 2(c). The photocurrent is caused by excitation of the electron–hole pairs under UV light when the photon energy is larger than the band gap. The low photocurrent at 365 nm is possibly due to the direct excitation of carriers from defect states in the band gap to the conduction band. The sensitivity decreases at shorter wavelength (254 nm) even though the absorption coefficient for this wavelength is high. This is because these higher-energy photons are absorbed at or near the surface of the semiconductor, where the photogenerated electron and hole pairs recombine at a much higher rate than in the bulk region. Thus, the photogenerated electrons and holes contribute less to the photocurrent [25].

The photoconductance of the WO_3 nanowires is also dependent on light intensity, as shown in Fig. 2(d) for illumination at 312 nm. It was found that the photocurrent (I_{ph}) can be fitted by a simple power law [8],

$$I_{ph} \propto P^{0.95} \quad (2)$$

where P is the intensity of the UV illumination. As the UV light intensity is relatively low, no saturation photocurrent can be observed in Fig. 2(d). The near-linear relationship suggests that the charge carrier photogeneration efficiency is approximately proportional to the number of photons absorbed by the nanowire. The hole trapped on the surface of the WO_3 nanowire do not absolutely release at low light intensity in our experiments, leading to no saturation in photocurrent.

The photoconductivity gain (G), defined as the number of electrons collected by electrodes due to absorption of a single photon, is a critical parameter for photoconductors. It can be expressed as

$$G = \frac{hvI_{ph}}{qPS(1-T)} \quad (3)$$

where I_{ph} is the photocurrent, S is the exposure area of the nanowire, T is the transmission of the UV light through the nanowire, v is the frequency of the light, and q is the electron charge [26, 27]. In Eq. (3), the surface reflection of light is neglected, and the quantum efficiency, defined as the number of photogenerated carriers excited by one photon, is assumed to be unity. In our experiment, $I_{ph} = 15$ nA, $P = 2.0$ mW/cm^2, $hv = 6.21 \times 10^{-19}$ J, $T = 0$, and $S = 6.28 \times 10^{-9}$ cm^2, so that the photoconductivity gain is about 4.6×10^3. This value is much higher than the gain of 1.3×10^3 reported for organic benzothiophene nanowires [25], and 1.0×10^2 for CdS nanoribbons [26], but still much smaller than that of 2.0×10^8 reported for ZnO nanowires [28]. The large gain could be caused by the following three factors: (1) the large surface-to-volume ratio; (2) the existence of deep level surface trap states in the WO_3 nanowires greatly prolonging the photocarrier lifetime; and (3) the reduced gap between the two electrodes shortening the carrier transit time. Consequently, a long lifetime and short transit time of photogenerated carriers cause a large gain [29].

Figure 3 shows the time response of the photocurrent to UV illumination at 312 nm with an intensity of 2 mW/cm^2. The photocurrent increases by a factor of 150 from 0.1 nA to 17.2 nA upon exposure. The reproducible response of the photocurrent (Fig. 3(a)) suggests the excellent stability of the device. It is worth mentioning that the time constant for the rise time (t_r) is always faster than the fall time (t_f) (Fig. 3(b)), which suggests that traps and other defect states are involved in this process.

Because of the high surface-to-volume ratio, the surface states can significantly affect the photogenerated carriers and, in turn, the transport and photoconductivity of the WO_3 nanowires. Oxygen molecules can be adsorbed on the oxide surface and capture the free electrons from the n-type WO_3 nanowire, so that a low-conductivity depletion layer is formed near the surface:

$$O_2(g) + e^- \rightarrow O_2^-(ad) \quad (4)$$

Under UV light illumination, electron–hole pairs are generated. The holes diffuse into the depletion region

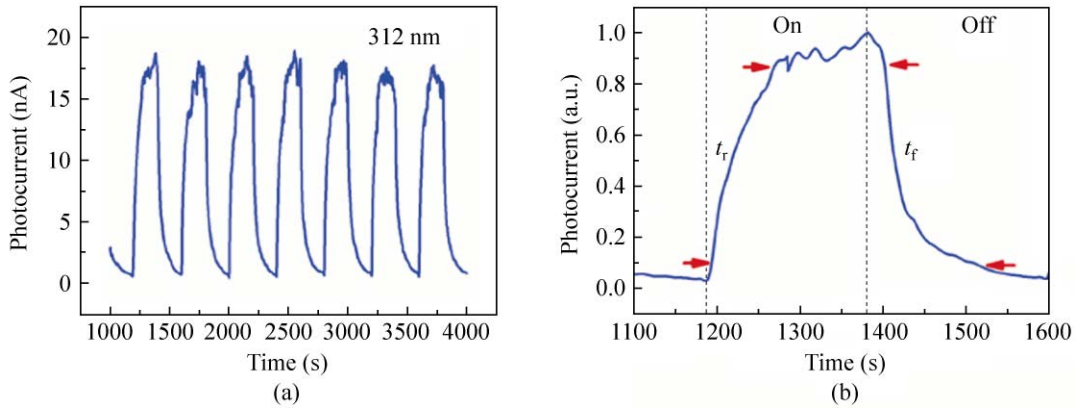

Figure 3 (a) Time response of the photocurrent from a single WO_3 nanowire to UV light (312 nm, 2 mW/cm^2), The bias voltage is 1 V. (b) Detailed view of typical time response spectrum, where the arrows indicate the 10% and 90% points to the peak value used for calculating the rise and fall time. t_r is the rise time and t_f is the fall time

and drift to the surface along the electric field and neutralize the adsorbed oxygen ions:

$$\text{hole}^+ + O_2^-(\text{ad}) + h\nu \rightarrow O_2(\text{g}) \quad (5)$$

Consequently, the adsorbed oxygen ions could desorb from the surface so that the extent of the low-conductivity depletion layer is reduced. The electrons are either collected at the electrodes or recombine with holes. This hole-trapping mechanism through oxygen adsorption and desorption on the surface of the WO_3 nanowires changes the density of the trap states on the surface, and thus enhances the WO_3 nanowire photoresponse.

To check for any possible surface effects on electron transport due to the atmosphere, we compared the dark currents of the WO_3 nanowires under vacuum (0.1 mbar) and in air as shown in Fig. 4(a). The dark conductance in a vacuum increases by a factor of 10 compared to that in air. In a vacuum, a small fraction of oxygen molecules can desorb from the surface of the WO_3 nanowire, leading to a small number of captured electrons being released from the near-surface depletion region.

After exposure to 312 nm UV light in a vacuum, the photocurrent increased to ~50 nA (Fig. 4(b)), higher than the photocurrent in air under the same incident light intensity. This increase in the photocurrent can be attributed to the increase in the density of photogenerated carriers because of the long lifetime of the electrons due to there being less oxygen readsorption in the oxygen-deficient environment. Actually, under UV illumination in a vacuum, more oxygen ions can be desorbed from the surface of the WO_3 nanowire, leading to a narrower depletion width and a higher photocurrent than in air. When the UV light is switched off in vacuum, the small number density of the recombination centers and the reduced depletion region naturally leads to a large persistent current. Therefore, the current did not return to the original dark level even after 12 h. A periodic change can be observed when the atmosphere is switched between O_2 and N_2 at atmospheric pressure (Fig. 4(c)). However, the current decreases only slightly when moisture is introduced into the chamber compared to the O_2 environment, as shown in Fig. 4(d). Therefore, we conclude that reduction of the photocurrent is mainly caused by the adsorption of oxygen, rather than moisture in the air. This result is consistent with the bonding of oxygen with surface defect sites being stronger than that of water [30].

In summary, we find that hexagonal WO_3 nanowires are very sensitive to UV illumination. An increase of more than two orders of magnitude in the conductance is obtained under UV illumination at 312 nm with an intensity of 2 mW/cm^2. The high photoconductivity gain of 4.6×10^3 suggests that the WO_3 nanowires can be used as the sensing element in UV photodetectors with a very high sensitivity. Adsorption of oxygen molecules on the surface of the WO_3 nanowires has a significant influence on both dark conductance and

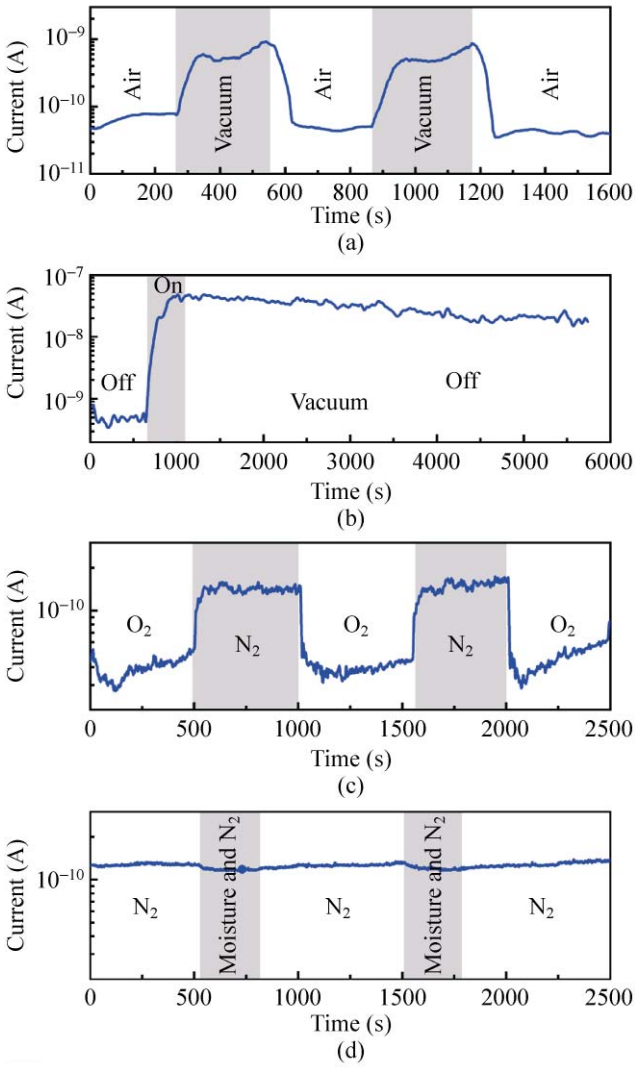

Figure 4 The response of current from a single WO_3 nanowire device under different atmospheres: (a) in vacuum and in air; (b) the photoresponse in vacuum with 312 nm UV illumination; (c) pure N_2 and O_2 at atmospheric condition; and (d) pure N_2 and moisture mixed with N_2, respectively. In the measurements, the bias voltage is 1 V, and the vacuum is 0.1 mbar

photoconductance. In a vacuum, the WO_3 nanowires are much more sensitive to UV light and the UV light-induced conductance decays at a much slower rate than in air. These results will open up new possibilities for using WO_3 nanowires in the fabrication of biosafe nanodevices such as high-performance ultraviolet B (UVB) radiation sensors, and also in future biological sensors and optoelectronic applications such as optical keys or optical memory, and further exploration in this direction is highly desirable.

References

[1] Blank, T. V.; Gol'dberg, Yu. A. Semiconductor photoelectric converters for the ultraviolet region of the spectrum. *Semiconductors* **2003**, *37*, 999–1030.

[2] Cui, H. T.; Zayat, M.; Parejo, P. G.; Levy, D. Highly efficient inorganic transparent UV-protective thin-film coating by low temperature sol–gel procedure for application on heat-sensitive substrates. *Adv. Mater.* **2008**, *20*, 65–68.

[3] Kong, J.; Franklin, N. R.; Zhou, C. W.; Chapline, M. G.; Peng, S.; Cho, K.; Dai, H. J. Nanotube molecular wires as chemical sensors. *Science* **2000**, *287*, 622–625.

[4] Cui, Y.; Wei, Q. Q.; Park, H. K.; Lieber, C. M. Nanowire nanosensors for highly sensitive and selective detection of biological and chemical species. *Science* **2001**, *293*, 1289–1292.

[5] Comini, E.; Faglia, G.; Sberveglieri, G.; Pan, Z.; Wang, Z. L. Stable and highly sensitive gas sensors based on semiconducting oxide nanobelts. *Appl. Phys. Lett.* **2002**, *81*, 1869–1871.

[6] Huang, J. X.; Virji, S.; Weiller, B. H.; Kaner, R. B. Polyaniline nanofibers: Facile synthesis and chemical sensors. *J. Am. Chem. Soc.* **2003**, *125*, 314–315.

[7] Calarco, R.; Marso, M.; Richter, T.; Aykanat, A. I.; Meijers, R.; Hart, A. V. D.; Stoica, T.; H. Lüth, H. Size-dependent photoconductivity in MBE-grown GaN–nanowires. *Nano Lett.* **2005**, *5*, 981–984.

[8] Kind, H.; Yan, H.; Messer, B.; Law, M.; Yang, P. D. Nanowire ultraviolet photodetectors and optical switches. *Adv. Mater.* **2002**, *14*, 158–160.

[9] Feng, P.; Zhang, J. Y.; Li, Q. H.; Wang, T. H. Individual β-Ga_2O_3 nanowires as solar-blind photodetectors. *Appl. Phys. Lett.* **2006**, *88*, 153107.

[10] Zhang, J. Y.; Chen, Y. X.; Guo, T. L.; Lin, Z. X.; Wang, T. H. Sub-band-gap photoconductivity of individual α-Si_3N_4 nanowires. *Nanotechnology* **2007**, *18*, 325603.

[11] Sanrato, C.; Odziemkowski, M.; Ulmann, M.; Augustynski, J. Crystallographically oriented mesoporous WO_3 films: Synthesis, characterization, and applications. *J. Am. Chem. Soc.* **2001**, *123*, 10639–10649.

[12] Li, Y. B.; Bando, Y. S.; Golberg, D. Quasi-aligned single-crystalline $W_{18}O_{49}$ nanotubes and nanowires. *Adv. Mater.*

2003, *15*, 1294–1296.

[13] Solis, J. L.; Saukko, S.; Kish, L.; Granqvist, C. G.; Lantto, V. Semiconductor gas sensors based on nanostructured tungsten oxide. *Thin Solid Films* **2001**, *391*, 255–260.

[14] Huang, K.; Jia, J. F.; Pan, Q. T.; Yang, F.; He, D. Y. Optical, electrochemical and structural properties of long-term cycled tungsten oxide films prepared by sol–gel. *Physica B* **2007**, *396*, 164–168.

[15] Livage, J.; Ganguli, D. Sol–gel electrochromic coatings and devices: A review. *Sol. Energy Mater. Sol. Cells* **2001**, *68*, 365–381.

[16] Rout, C. S.; Govindraj, A.; Rao, C. N. R. High-sensitivity hydrocarbon sensors based on tungsten oxide nanowires. *J. Mater. Chem.* **2006**, *16*, 3936–3941.

[17] Tao, T.; Yao, J. N. Photochromic materials based on tungsten oxide. *J. Mater. Chem.* **2007**, *17*, 4547–4557.

[18] Feng, M.; Pan, A. L.; Zhang, H. R.; Li, Z. A.; Liu, F.; Liu, H. W.; Shi, D. X.; Zou, B. S.; Gao, H. L. Strong photo-luminescence of nanostructured crystalline tungsten oxide thin films. *Appl. Phys. Lett.* **2005**, *86*, 141901.

[19] Wang, S. J.; Lu, W. J.; Cheng, G.; Cheng, K.; Jiang, X. H.; Du, Z. L. Electronic transport property of single-crystalline hexagonal tungsten trioxide nanowires. *Appl. Phys. Lett.* **2008**, *94*, 263106.

[20] Huang, K.; Pan, Q. T.; Yang, F.; Ni, S. B.; Wei, X. C.; He, D. Y. Controllable synthesis of hexagonal WO_3 nano-structures and their application in lithium batteries. *J. Phys D: Appl. Phys.* **2008**, *41*, 155417.

[21] Zhou, J.; Ding, Y.; Deng, S. Z.; Gong, L.; Xu, N. S.; Wang, Z. L. Three-dimensional tungsten oxide nanowire networks. *Adv. Mater.* **2005**, *17*, 2107–2110.

[22] Choi, H. G.; Jung, Y. H.; Kim, D. K. High quality tungsten oxide nanowires: Synthesis and characterization. *J. Am. Ceram. Soc.* **2005**, *88*, 1684–1686.

[23] Li, X. L.; Liu, J. F.; Li, Y. D. Large-scale synthesis of tungsten oxide nanowires with high aspect ratio. *Inorg. Chem.* **2003**, *42*, 921–924.

[24] Butler, M. A. Photoelectrolysis and physical properties of the semiconducting electrode WO_2. *J. Appl. Phys.* **1977**, *48*, 1914–1920.

[25] Amalnerkar, D. P. Photoconducting and allied properties of CdS thick films. *Mater. Chem. Phys.* **1999**, *60*, 1–21.

[26] Zhou, Y.; Wang, L.; Wang, J.; Pei, J.; Cao, Y. Highly sensitive, air-stable photodetectors based on single organic sub-micrometer ribbons self-assembled through solution orocessing. *Adv. Mater.* **2008**, *20*, 3745–3749.

[27] Jie, J. S.; Zhang, W. J.; Jiang, Y.; Meng, X. M.; Li, Y. Q.; Lee, S. T. Phtotoconductive characteristics of single-crystal CdS nanoribbons. *Nano Lett.* **2006**, *6*, 1887–1892.

[28] Soci, C.; Zhang, A.; Xiang, B.; Dayeh, S. A.; Aplin, D. P. R.; Park, J.; Bao, X. Y.; Lo, Y. H.; Wang, D. ZnO nanowire UV photodetector with high internal gain. *Nano Lett.* **2007**, *7*, 1003–1007.

[29] Bube, R. H. *Photoconductivity of Solids*; Wiley: New York, 1960; pp 461–469.

[30] Ahn, S. E.; Lee, J. S.; Kim, H.; Kim, S.; Kang, B. H.; Kim. K. H.; Kim, G. T. Photoresponse of sol-gel-synthesized ZnO nanorods. *Appl. Phys. Lett.* **2004,** *84*, 5022–5024.